

Graph-Based Topology Correction for Brain Cortex Segmentation

Xiao Han¹, Chenyang Xu², Ulisses Braga-Neto¹, and Jerry L. Prince¹

¹ Center for Imaging Science, Johns Hopkins University, Baltimore MD 21218, USA
xhan@iron.ece.jhu.edu, ulisses@ece.jhu.edu, prince@jhu.edu

² Siemens Corporate Research, Princeton, NJ 08540, USA
cxu@scr.siemens.com

Abstract. Reconstructing a topologically correct representation of the brain cortex surface from magnetic resonance images is important in several medical and neuroscience applications. Most previous methods have either made drastic changes to the underlying anatomy or relied on hand-editing. Recently, a new technique due to Shattuck and Leahy yields a fully-automatic procedure with little distortion of the underlying segmentation. The present paper can be considered as an extension of this approach to include arbitrary cut directions and arbitrary digital connectivities. A detailed analysis of the method's performance on 15 magnetic resonance brain images is provided.

1 Introduction

Automatic reconstruction of the brain cortical surface from magnetic resonance (MR) images is an important goal in medicine and neuroscience. In recent years, there has been a considerable effort in developing methods for this purpose [3, 4, 10, 11]. Because of imaging noise, the partial volume effect, image intensity inhomogeneities, and the highly convoluted nature of the brain cortex itself, it is difficult to produce a representation that is both accurate and has the correct topology. The major topological difficulty is the presence of one or more handles within the surface, which prevents the reconstructed surface from being correctly mapped to the plane or the sphere [4, 12].

Manual editing has been one of the most widely employed techniques to guarantee both accuracy in surface representation and correct topology [3, 4, 10]. Several automatic techniques have also been proposed to generate a topologically correct representation of the WM/GM surface, including the well-known *homotopic region growing model* [5] and its dual procedure [1]. The problem with the latter approaches is that the topology might be corrected in very unpredictable ways; for example, causing “cuts” across the whole brain. Another approach involving successively filtering the white matter followed by an isosurface algorithm [11] produced the correct topology, but the final surface could be far away from the truth.

Recently, a new approach to topology correction was introduced by Shattuck and Leahy [7, 8]. Instead of region-growing or global filtering, this approach

examines the connectivity of the binary white matter segmentation to find regions that give rise to incorrect topology, and carefully edits them to correct the topology. Their method is elegant and effective and there is little room for improvement. However, the authors acknowledge that their “cuts” are not natural since they can only be oriented along the cartesian axes. They also describe a particular topological problem in which “slice duplication” is required. Finally, their approach requires 6-connectivity of the digital object, and cannot be used with any other digital connectivity.

In this paper, we develop a new algorithm, which we refer to as the *graph-based topology correction filter* (GTCF), that removes all handles from a binary object. Our method is intrinsically three-dimensional and “cuts” are not forced to be oriented along cardinal axes. It does not require the introduction of slice duplication, and any (consistent) digital connectivity definition can be used. A final distinction of our approach with that of Shattuck and Leahy is that the correct topology can be assured through application of either foreground or background filters alone, resulting in either handles being cut or tunnels being filled exclusively. In the following sections, we give necessary background, describe our method, and provide experimental results that show the overall characteristics and performance of this method.

2 Background

Although we desire a topologically correct surface, the correction is applied on the volume data and an isosurface algorithm is used to generate the surface itself. In this section we review some notions from 3D discrete topology, isosurface algorithms, and the topology of digital meshes. These three areas provide key ingredients in our approach.

2.1 3D Discrete Topology. A 3D digital image $V \subset Z^3$ is defined as a cubic array of lattice points. We follow the conventional definition of *n-neighborhood* and *n-adjacency*, where $n \in \{6, 18, 26\}$. We denote the *n-neighborhood* of a point x by $N_n(x)$, and the neighborhood of x with x removed by $N_n^*(x)$.

An *n-path of length $l > 0$* from p to q in X means a sequence of distinct points $p = p_0, p_1, \dots, p_l = q$ of X such that p_i is *n-adjacent* to p_{i+1} , $0 \leq i < l$. Two points $p, q \in X$ are *n-connected* if there exists an *n-path* from p to q in X . A set of points X is called *n-connected* if every two points $p, q \in X$ are *n-connected* in X . An *n-connected component* of a set of points X is a non-empty *n-connected* subset of X that is not *n-adjacent* to any other point in X . We denote the set of all *n-connected components* of X by $\mathcal{C}_n(X)$.

In order to avoid a connectivity paradox, different connectivities, n and \bar{n} , must be used in a binary image comprising an object (foreground) X and a background \bar{X} . For example, (6,18) and (6,26) are two pairs of compatible connectivities. Following [2], we distinguish the 6-connectivity associated with the 18-connectivity by 6^+ -connectivity. The following definitions are from [2]:

Definition 1 (Geodesic Neighborhood) Let $X \subset V$ and $x \in V$. The geodesic neighborhood of x with respect to X of order k is the set $N_n^k(x, X)$ defined recursively by: $N_n^1(x, X) = N_n^*(x) \cap X$ and $N_n^k(x, X) = \cup \{N_n(y) \cap N_{26}^*(x) \cap X, y \in N_n^{k-1}(x, X)\}$.

Definition 2 (Topological Numbers) Let $X \subset V$ and $x \in V$. The topological numbers relative to the point x and the set X are: $T_6(x, X) = \#C_6(N_6^2(x, X))$, $T_{6+}(x, X) = \#C_6(N_6^3(x, X))$, $T_{18}(x, X) = \#C_{18}(N_{18}^2(x, X))$, and $T_{26}(x, X) = \#C_{26}(N_{26}^1(x, X))$, where $\#$ denotes cardinality of a set.

2.2 Isosurface Algorithm. In this paper, we use a modified marching cubes (MC) algorithm [6] to produce a surface representation of a binary digital object (1=object, 0=background). As pointed out in [6], by incorporating both the face and the body saddle points, the MC algorithm can produce a surface consistent with trilinear interpolation and free from topological paradoxes. In this case, we have further shown that, for binary objects, setting the isovalue to be less than 0.25 yields 26-connectivity; setting the isovalue between 0.25 and 0.5 yields 18-connectivity; and setting the isovalue above 0.5 yields 6-connectivity.

2.3 Topology of Surface Meshes. The number of handles on a surface is called the *genus* of the surface, and is given by $g = 1 - \chi/2$, where χ is the *Euler number*. The Euler number in turn can be computed using $\chi = V - E + F$, where V , E , and F are the number of vertices, edges, and faces, respectively, of the surface mesh. A surface is topologically equivalent to a sphere when $g = 0$; however, neither the Euler number nor the genus provides information about the size or location of a handle.

Given a topologically consistent isosurface algorithm, there is a one-to-one correspondence between the handles on a binary digital object with n -connectivity and that of its triangulated surface representation. We therefore check the topology of the object by computing the Euler number of its isosurface computed using the correct threshold.

3 Graph-based Topology Correction Filter

Our graph-based topology correction filter (GTCF) aims to remove all the handles in a binary volume consisting of a single connected foreground object with no cavities (which are easily removed by region-growing). GTCF can operate on the original volume or its complement, giving foreground and background filters respectively. Handles removed by a background filter correspond to tunnels filled in the original volume. Compatible connectivities must be used for the two filters, yielding an n -connectivity foreground filter and an \bar{n} -connectivity background filter. For simplicity, we describe the foreground filter with n -connectivity only, but the background filter is the same with n replaced by \bar{n} .

A block diagram of GTCF is shown in Fig. 1(a), and the basic idea is illustrated in Fig. 1(b). The method consists of four major steps, which are repeated at successively increasing scales until all handles or tunnels are removed. We now describe each step; some details are omitted due to lack of space.

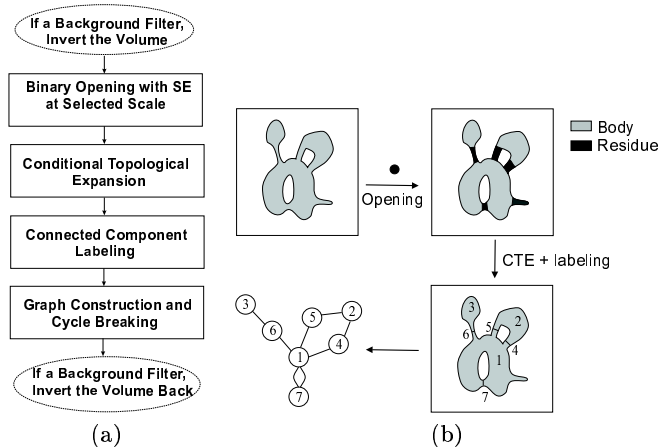


Fig. 1. Topology correction filter: (a) flowchart and (b) illustration.

3.1 Binary Morphological Opening. The morphological opening of an object F with a structuring element B removes all parts of F that are smaller than B , in the sense that they cannot contain any translated replica of B . We use morphological opening to detect handles at different scales. We call the structuring element (SE) used at the smallest scale (scale 1) the *basic structuring element*. The SE at scale k is obtained by $k - 1$ successive dilations of the basic SE with itself. In practice, we use a digital ball of radius one — i.e., an 18-neighborhood plus the center point — as the basic SE. The shape of the basic SE is not critical; for example, we could also use a 3D cross, which has only seven points.

As illustrated in Fig. 1(b), the opening operation divides the foreground object into two classes. Points that are in the resulting (opened) image are called *body* points, and points that are removed by the opening operator are called *residue* points.

3.2 Conditional Topological Expansion. On a complicated shape such as a white matter segmentation, morphological opening removes far more voxels than just those required to break the handles. The residue typically comprises many connected components, several of which are large, complicated shapes. Also, the opening can actually *create* handles in the body component. For these reasons, we cannot discard residue components at this stage in order to break handles. Instead, we introduce *conditional topological expansion* (CTE), which aims to transfer as many points as possible from the residue back to the body, without introducing handles.

Algorithm 1 (Conditional Topological Expansion (CTE)):

1. Find the set S of residue points that are n -neighbors of the body points X .
2. For each point $x \in S$, if $T_n(x, X) = 1$ then let $X \leftarrow X \cup x$.
3. If no point changed its label in Step 2, then stop; otherwise, go to Step 1.

The criterion in Step 2 involving the topological number is Property 5 in Bertrand [2].

It guarantees that the set $x \cup X$ has no more handles than X . Thus, CTE can fill handles created by morphological opening, but cannot create new handles.

3.3 Connected Component Labeling. After CTE, the remaining residue pieces form thin “cuts” that separate body components, as depicted in the third diagram of Fig. 1(b). To prepare for a graph-based analysis of topology, it is necessary to label all the connected components. The basic steps are as follows.

First, we compute the connected components of the body using n -connectivity. We then computed the topological number of each residue point with respect to each body component. Residue points that are connected to the same body component more than once form simple handles, and are immediately removed.

Second, we compute the connected components of the remaining residue and calculate the number of connections between each residue connected component (RCC) and its adjacent body connected components (BCCs). It turns out that this analysis is subtle, because certain handle configurations cannot be detected during the subsequent graph-based analysis and must be addressed here.

Finally, we seek to merge RCCs whenever possible. This can be done when body and residue components together form a solid object without any handles.

3.4 Graph Construction and Cycle Breaking. Finally, we build a graph whose nodes represent the RCCs and BCCs and whose edges represent the connections between the RCCs and BCCs, as shown in Fig. 1(b). We then search for cycles in this graph using a depth-first search algorithm. When a cycle is detected, we break it by removing the RCC with the smallest size (number of voxels) among all the RCCs in the cycle. Whenever a cycle is broken, it is necessary to restart the algorithm at the starting node of that cycle so that the modified graph is correctly traversed.

After all the cycles are broken, we construct a new object by putting together all the remaining RCCs and the BCCs. This is the output of the topology correction filter. If a background filter is used, the new volume is inverted back. We then apply our marching cubes algorithm with an isovalue chosen in the correct range to reflect the desired connectivity. If its genus is zero, then the topology of the new volume is correct, and we stop (and compute the final surface using MC with the appropriate isovalue). Otherwise, we either switch to the opposite filter at the same scale (if not already applied) or increase the scale of the current filter, and continue the topology correction on the new volume.

4 Results

The object depicted in Fig. 2(a) illustrates the results of applying a foreground filter ($n = 18$) and a background filter ($\bar{n} = 6^+$) to the same handle. The foreground filter removed the handle by breaking it along a thin part, while the background filter filled the tunnel with a thin sheet. In both cases, the “cuts” are small and clearly not oriented in cartesian directions.

We applied our proposed topology correction filter to 15 MR brain image volumes obtained from the Baltimore Longitudinal Study on Aging [9]. The typical

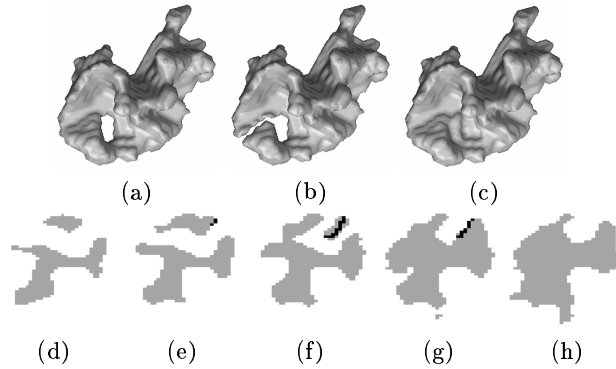


Fig. 2. (a) A handle taken from an actual white matter volume. The result of using (b) a foreground filter and (c) a background filter. (d)-(h): consecutive slices showing the cut made by the foreground filter.

image size after cropping the background was $140 \times 200 \times 160$. All images were preprocessed and segmented using an updated version of the method described in [11]. The filter was then applied to all 15 brain volumes in a sequence alternating between foreground (F) and background (B) filtering, and then increasing in scale. We used $n = 18$ and $\bar{n} = 6^+$, and the basic SE was an 18-connected digital ball. Tables 1 and 2 show the original genus (number of handles) in the white matter isosurface and the genus after each filter stage from top to bottom. The bottom row of each table shows the number of voxels that were changed from either foreground to background or background to foreground for each brain.

Comparing the results of the two tables, we see that the change to the volume is less if we apply the background filter first. The reason is that the background filter uses 6-connectivity while the foreground is 18; therefore, narrower “swaths” can be used to break handles. On the other hand, beginning with the foreground filter yields a faster reduction in the number of handles. From the results, it is also shown that the ratio of the number of voxels changed to the number of handles in the original volume is around 3, which is comparable to the results reported in [7, 8].

5 Conclusion

We have developed and evaluated an automatic method called GTCF to remove handles in 3D digital images. GTCF is intrinsically three-dimensional, does not require the introduction of half-thickness slices as in [7, 8], any consistent digital connectivity can be used, and it can optionally be used to exclusively cut handles or fill tunnels if desired. It has been shown to work well on 15 magnetic resonance segmented volumes.

Table 1. Genus and Number of Voxels Changed Using a F-B Sequence.

Brain	S1	S2	S3	S4	S5	S6	S7	S8	S9	S10	S11	S12	S13	S14	S15
Original	724	955	1376	744	1031	776	562	886	688	825	986	597	1944	1280	801
f1	4	5	19	0	5	5	1	11	4	0	5	5	16	9	4
b1	0	0	1	0	2	0	0	2	0	0	0	1	0	0	0
f2	0	0	0	0	0	0	0	0	0	0	0	0	0	0	0
b2	0	0	0	0	0	0	0	0	0	0	0	0	0	0	0
Changes	2398	3284	4407	1973	3081	1872	1563	2584	2023	2118	2691	1618	6416	3678	2165

Table 2. Genus and Number of Voxels Changed Using a B-F Sequence.

Brain	S1	S2	S3	S4	S5	S6	S7	S8	S9	S10	S11	S12	S13	S14	S15
Original	724	955	1376	744	1031	776	562	886	688	825	986	597	1944	1280	801
b1	46	32	32	40	31	24	16	36	26	23	20	17	57	36	21
f1	0	0	0	0	0	1	0	0	1	0	0	0	0	0	0
b2	0	0	0	0	0	1	0	0	1	0	0	0	0	0	0
f2	0	0	0	0	0	0	0	0	0	0	0	0	0	0	0
Changes	1456	2054	2846	1509	3200	1728	1104	2141	1359	1555	1807	1135	4213	2653	1589

Acknowledgments. We thank Drs. Sinan Batman, John Goutsias, Susan Resnick, and Dzung Pham for their contributions. This work was supported in part by NSF/ERC grant CISST#9731748 and NIH/NINDS grant R01NS37747.

References

1. Z. Aktouf, G. Bertrand and L. Perroton, "A 3D-hole closing algorithm," in *6th Int. Workshop on Discrete Geometry for Computer Imagery*, 36–47, 1996.
2. G. Bertrand, "Simple points, topological numbers and geodesic neighborhoods in cubic grids," *Patt. Recog. Lett.*, 15:1003–1011, 1994.
3. G. Carman, H. Drury, and D. Van Essen, "Computational methods for reconstructing and unfolding the cerebral cortex," *Cerebral Cortex*, 5:506–517, 1995.
4. A. Dale, B. Fischl, and M. Sereno, "Cortical surface-based analysis I & II," *NeuroImage*, 9:179–207, 1999.
5. J.-F. Mangin, V. Frouinh, J. Regis, and J. Lopez-Krahe, "From 3D magnetic resonance images to structural representations of the cortex topography using topology preserving deformations," *J. Math. Imag. Vision*, 5:297–318, 1995.
6. B. Natarajan, "On generating topologically consistent isosurfaces from uniform samples," *The Visual Computer*, 11(1):52–62, 1994.
7. D. Shattuck and R. Leahy, "Topological refinement of volumetric data," in *Proc. of the SPIE*, 3661:204–213, Feb. 1999.
8. D. Shattuck and R. Leahy, "Topologically constrained cortical surfaces from MRI," in *Proc. of the SPIE*, 3979:747–758, Feb. 2000.
9. S. M. Resnick, A. F. Goldszal, C. Davatzikos, S. Golski, M. A. Kraut, E. J. Metter, R. N. Bryan, and A. B. Zonderman, "One-year age changes in MRI brain volumes in older adults", *Cerebral Cortex*, 10(5): 464–472, 2000.
10. P. Teo, G. Sapiro, and B. Wandell, "Creating connected representations of cortical GM for functional MRI visualization", *IEEE Trans. Med. Imag.*, 16:852–863, 1997.
11. C. Xu, D. Pham, M. Rettmann, D. Yu, and J. Prince, "Reconstruction of the human cerebral cortex from MR images," *IEEE Trans. Med. Imag.*, 18(6):467–480, 1999.
12. D. Van Essen and J. Maunsell, "Two dimensional maps of cerebral cortex," *J. of Comparative Neurology*, 191:255–281, 1980.